Single-block rockfall dynamics inferred from seismic signal analysis

Clément Hibert[1], Jean-Philippe Malet[1], Franck Bourrier[2], Floriane Provost[1], Frédéric Berger[2], Pierrick Bornemann[1], Pascal Tardif[2], and Eric Mermin[2]

[1]Institut de Physique du Globe de Strasbourg - CNRS UMR 7516, University of Strasbourg/EOST, 5 rue Descartes, 67084 Strasbourg, France
[2]Institut national de recherche en sciences et technologies pour l'environnement et l'agriculture (IRSTEA), 2 Rue de la Papeterie, 38402 Saint-Martin-d'Hères, France

Correspondence to: Clément Hibert (hibert@unistra.fr)

Abstract.

Seismic monitoring of mass movements can significantly help to mitigate the associated hazards, however the link between event dynamics and the seismic signals generated is not completely understood. To better understand these relationships, we conducted controlled releases of single blocks within a soft-rock (black marls) gully of the Rioux-Bourdoux torrent (French Alps). 28 blocks, with masses ranging from 76 kg to 472 kg, were used for the experiment. An instrumentation combining video cameras and seismometers was deployed along the traveled path. The video cameras allow reconstructing the trajectories of the blocks and estimating their velocities at the time of the different impacts with the slope. These data are compared to the recorded seismic signals. As the distance between the falling block and the seismic sensors at the time of each impact is known, we were able to determine the associated seismic signal amplitude corrected from propagation and attenuation effects. We compared the velocity, the potential energy lost, the kinetic energy and the momentum of the block at each impact to the true amplitude and the radiated seismic energy. Our results suggest that the amplitude of the seismic signal is correlated to the momentum of the block at the impact. We also found relationships between the potential energy lost, the kinetic energy and the seismic energy radiated by the impacts. Thanks to these relationships, we were able to retrieve the mass and the velocity before impact of each block directly from the seismic signal. Despite high uncertainties, the values found are close to the true values of the masses and the velocities of the blocks. These relationships also provide new insights to understand the source of high-frequency seismic signals generated by rockfalls.

1 Introduction

Understanding the dynamics of rockfalls and other mass movements is critical to mitigate the associated hazards but is very difficult because of the limited number of observations of natural events. With the densification of the global, regional and local seismometer networks, seismic detection of gravitational movements is now possible. The continuous recording ability of seismic networks allows a reconstruction of the gravitational activity at unprecedented time scale and the monitoring of unstable slopes (e.g. Amitrano et al., 2005; Helmstetter and Garambois, 2010; Levy et al., 2011; Burjánek et al., 2012; Panzera et al., 2012; Galea et al., 2014). More than the detection of these events, recent advances allow determining the dynamics

of the largest landslides on Earth from the very low-frequency seismic waves they generate. Inversion and modeling of the long-period seismic waves permits to infer the force imparted by these catastrophic events on Earth, and to deduce dynamic parameters (acceleration, velocity, trajectory) as well as their mass (Favreau et al., 2010; Schneider et al., 2010; Moretti et al., 2012; Ekström and Stark, 2013; Allstadt, 2013; Yamada et al., 2013; Hibert et al., 2014a, c). However, these approaches are limited by the size of the events. Only the largest landslides will generate the long-period seismic waves used in the inversion and the modeling methods. Moreover these events constitute only a small proportion of the landslides that occur worldwide.

In recent years, a new approach based on the analysis of the high-frequency seismic signal has been proposed. High-frequency seismic waves are generated independently of the size of the event, and can be recorded if seismometers are close enough to the source. Hence, this allows a seismic detection of the events that do not generate long-period seismic waves (e.g. Deparis et al., 2008; Helmstetter and Garambois, 2010; Dammeier et al., 2011, 2016; Hibert et al., 2011, 2014b; Clouard et al., 2013; Chen et al., 2013; Burtin et al., 2013; Tripolitsiotis et al., 2015; Zimmer and Sitar, 2015). The limitation of this approach is that high-frequency seismic waves are more prone to be influenced by propagation effects (attenuation, dispersion, scattering) and, more importantly, that the source of the high-frequency seismic waves associated with gravitational instabilities is not well understood yet.

Studies have shown that several landslide properties can be linked to features of the high-frequency seismic signals. In some cases, it has been observed that the landslide volumes is correlated to the amplitude (Norris, 1994; Dammeier et al., 2011) or to the radiated seismic energy of the high-frequency signals (Hibert et al., 2011; Yamada et al., 2012). Other studies have shown that the high-frequency seismic signals can also carry information on landslide dynamics. Schneider et al. (2010) have determined with numerical modeling that a good correlation exists between the short-period seismic-signal envelope, the modeled friction work rate and the momentum (product of the mass and the velocity) for two rock-ice avalanches. The model-based approach proposed by Levy et al. (2015) has shown that a correlation can be found between the modeled force and the power of the short-period seismic signal for rockfalls that occurred at the Soufrière Hills volcano on Montserrat Island. Hibert et al. (2017) have demonstrated that, for 11 large landslides that occurred worldwide, the bulk momentum controls at the first order the amplitude of the envelope of the generated seismic signals filtered between 3 Hz and 10 Hz. These authors also demonstrated that the maximum amplitude of the seismic signal, corrected from propagation effects, is quantitatively correlated with the bulk momentum. These results are important as they open the perspective to quantify the landslide dynamics, independently of their size, and directly from the seismic signals they generate (i.e. without inversion or modeling). Being capable of quantifying the landslide properties directly from the seismic signals they generate is critical for the development of future methods aimed at their real-time detection and characterization using high-frequency seismic signals. However, before considering an operational implementation of such methods, we need to better understand the source of the high-frequency seismic radiations generated and their links with the landslide dynamics.

One of the assumptions that emerge from these studies to explain the link between the landslide dynamics and the high-frequency seismic signal features is that this relationship can potentially originates from small-scale processes within the landslide mass, and between the landslide mass and the substrate. The impulse imparted to the solid Earth by a bouncing particle within a granular flow might be proportional to its dynamics, and the amplitude of the seismic wave might be proportional to

the magnitude of the impulse. However, this assumption raises an important issue: what is the link between the dynamics of a single bouncing particle (a rock for example) and the seismic signal generated?

Theoretical developments, laboratory and field experiments were conducted by Farin et al. (2015) to address this issue. These authors have shown that the mass and the speed of an impactor can be related to the radiated elastic energy and to the spectrum of the signal, following analytic developments based on the Hertz theory of impact (Hertz, 1882). However, the field experiment conducted showed that, in this case, these simple relationships did not perform well to quantify the velocity and the mass of single rocks from the seismic signal it generates. Difficulties to synchronize the seismic signals with direct observations and the use of a seismometer that was not capable to record the high-frequency energy of the generated seismic waves might explain why the analytic relationships were not confirmed by this experiment.

In this study we propose a new field experiment of controlled releases of single blocks to investigate the relationships between block properties and dynamics, and the features of the seismic signals generated by impacts with the slope. We deployed several short-period and broadband seismic stations to record the high-frequency seismic signal generated at each impact. The trajectory of each block is reconstructed with video cameras that were synchronized with the seismometers. The seismic signal processing allowed us inferring the amplitude of the seismic signal at the source, corrected from propagation effects, and the seismic energy radiated by the impacts. We then compare the features of the seismic signal of each impact to the dynamics and the properties of the released block.

2 The Rioux-Bourdoux experiment

The Rioux-Bourdoux controlled releases experiment focus was to study the seismic signal of single-block rockfalls on unconsolidated soft-rock, which is highly attenuating for seismic waves. The Rioux-Bourdoux is a torrent located in the French Alps, approximately 4 km north of the town of Barcelonnette (France). The slopes surrounding the torrent consist of Callovo-Oxfordian black-marls and are representative of the slope morphology of marly facies observed in south-east France. Due to the high erosion susceptibility of black marls numerous steep gullies have formed on these slopes.

We conducted the releases within one of these gullies (Figure 1a and b). The advantage of launching the blocks in a gully is that for every block the traveled path is roughly the same. Moreover, the steepness of the gullies that developed in black-marls allows the block to rapidly reach a high velocity. The travel path had a length of approximately 200 m and slope angles ranging from ~ 45 degrees on the upper part of the slope to ~ 20 degrees on the terminal debris cone. 28 blocks with masses ranging from 76 to 472 kg were manually launched.

Two video cameras (Sony alpha7 - 25 frame per seconds) were deployed at the base of the gully, close to the torrent. Ground-control points were marked for visual recognition on the videos and their 3D coordinates were measured by Global Navigation Satellite System (GNSS). A reference Digital Elevation Model (DEM) at a spatial resolution of 0.5 m was built from terrestrial LIDAR acquisitions (Figure 1c). The time of the cameras was set to be synchronous with the seismic sensors time (GPS). The seismic network was composed of 1 broadband seismometer (CMG40T - sampling frequency 100 Hz) located north of

the gully, and an antenna of 4 short-period seismometers (one 3 component and three with 1 vertical component - sampling frequency 1000 Hz) located south of the gully (Figure 1c).

3 Methods

3.1 Trajectory reconstruction and dynamic parameters estimation

5   To reconstruct the trajectory, the impacts of each block were manually picked on the frames of the videos. Thanks to the control points, the frames of the videos were projected on the DEM. Hence, once an impact was identified on the frame, the position of the pixel was reported on the DEM, which gave the true position of the impact. This processing was repeated for the two cameras, which gave an estimate of the uncertainties on the determination of the position and the time of the impact. The velocity just before impact was derived from the block trajectory and the duration of block flight before impact. The kinetic

10 energy was computed as:

$$E_k = \frac{1}{2}mV^2, \tag{1}$$

with m the mass of the block and V the velocity before impact. We also determined the potential energy lost during the block flight before impact from the difference of altitude of the block between two impacts, inferred from the reconstructed trajectory, as:

15 $$E_p = mg(h_{t_1} - h_{t_2}), \tag{2}$$

with g the gravitational acceleration, and h_{t_1} and h_{t_2} the altitudes of the block at the impacts that occurred at the two successive times t_1 and t_2. Unfortunately, the resolution of the cameras and the complex dynamics of the blocks during the first seconds of propagation did not allow us to identify clearly the impacts on the upper part of the slope. However the trajectories of the blocks on the lower part of the slope were well constrained, with an average uncertainty on the inferred

20 velocity of the blocks before impacts of $0.95\,\mathrm{m\,s^{-1}}$ for velocities with values comprised between $6\,\mathrm{m\,s^{-1}}$ and $17\,\mathrm{m\,s^{-1}}$.

3.2 Seismic signal processing

Several authors have shown that the seismic waves generated by gravitational instabilities are dominated by surface waves (e.g. Deparis et al., 2008; Hibert et al., 2011; Dammeier et al., 2011; Levy et al., 2015). These high-frequency seismic surface waves are subjected to strong propagation effects, especially in a highly attenuating medium such as black marls. Figure 2 shows the

25 seismic signals recorded for the launch of the block number 4. The attenuation is visible when comparing peaks in the seismic signal recorded at the station located on the upper part of the slope (Figure 2a) to the ones recorded at the station on the lower part of the slope (Figure 2c), for the same time. The amplitude of the peaks is clearly dependent on the distance between the
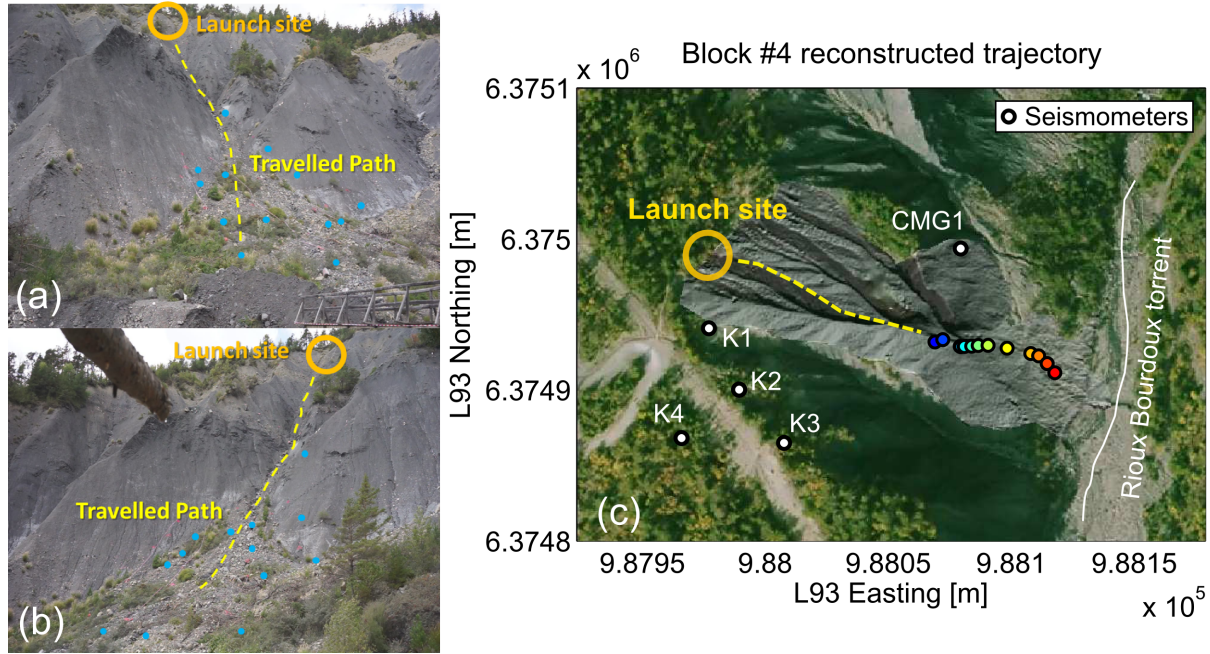
Figure 1. View from a) the first and b) the second video cameras deployed at the bottom of the slope. The ground control points are indicated by blue points. c) Trajectory reconstruction for block 4 on the DEM, built from LIDAR acquisition, superimposed on an orthophoto of the Rioux-Bourdoux slopes. Each point indicates the position of an impact and the color gradient represents the chronology of these impacts (blue for the first impact and red for the last one). K2 is a three-component short-period seismometer and K1, K3 and K3 are vertical-only seismometers. CMG1 is a broad-band seismometer.

impact and the seismic station. Moreover, Figure 2b shows the attenuation of the highest frequency with the distance of the source to the seismic station. To compare seismic signal features to the dynamic parameter of the rockfall, we have to correct these attenuation effects. Aki and Chouet (1975) proposed a simple attenuation law giving the amplitude $A(r)$ of a seismic surface wave recorded at a distance r as:

5
$$A(r) = \frac{1}{\sqrt{r}} A0 \times e^{-Br}. \tag{3}$$

If the distance between the station and the source is known, the computation of the amplitude at the source $A0$ is straightforward. However we have to determine the frequency dependent parameter B that accounts for the anelastic attenuation of seismic waves. If we consider r_i the distance between the source and station i and r_j the distance to station j, the apparent anelastic attenuation parameter B_{ij} is then:

10
$$B_{ij} = \frac{log(A(r_i)\sqrt{r_i}) - log(A(r_j)\sqrt{r_j})}{\sqrt{r_j} - \sqrt{r_i}}. \tag{4}$$

By combining Eq. (3) and Eq. (4), we can compute the amplitude at the source $A0$ for each pair of stations. This value is then averaged over all the pairs of stations, and the standard deviation gives an estimate of the uncertainty.
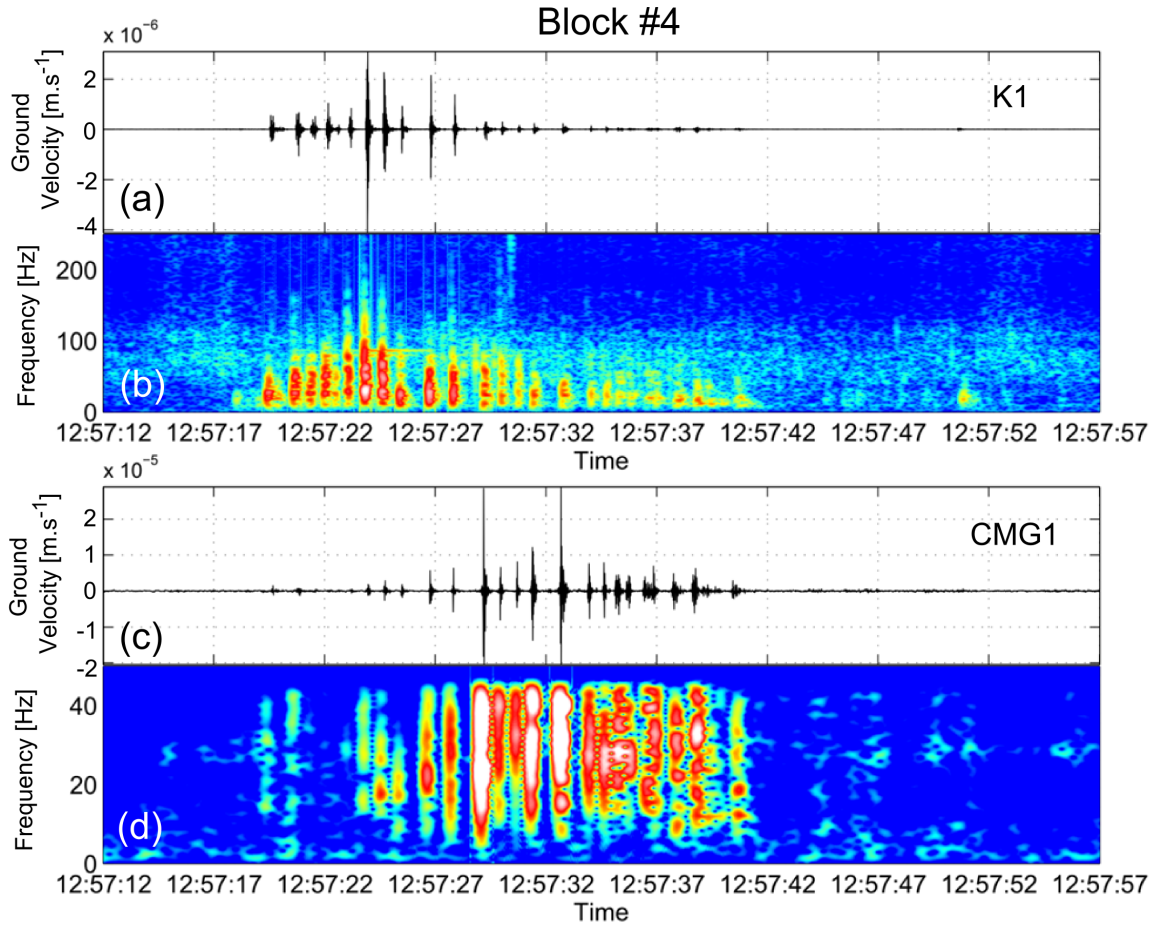

Figure 2. a) Signal recorded at the short-period station located on the upper part of the slope and b) corresponding spectrogram, generated by block number 4 (mass of 209 kg). c) Signal recorded at the broadband station located on the lower part of the slope and d) corresponding spectrogram, generated by block 4.

Another quantity that we want to compare to the dynamics of the block is the radiated seismic energy. The energy of a seismic surface wave can be computed as (Crampin, 1965):

$$E_s = \int_{t_i}^{t_f} 2\pi r D h c u_{env}(t)^2 e^{Br} dt, \tag{5}$$

5

with :

$$u_{env}(t) = \sqrt{u(t)^2 + Ht(u(t))^2}, \tag{6}$$

where Ht is the Hilbert transform of the seismic signal $u(t)$ used to compute the envelope $u_{env}(t)$, t_i and t_f the times of the beginning and the end of the seismic signal respectively, h the thickness and D the density of the layer through which the generated surface waves propagate, and c their phase velocity. The average velocity of surface waves in black-marls formations observed in the area of the Rioux Bourdoux torrent is approximately 300 m s^{-1} (Hibert et al., 2012; Gance et al., 2012), which, for seismic signal with central frequencies around $f = 20$ Hz as observed on Figure 2, gives a propagation depth h, computed as $h = c/f$, of ~ 15 m. The density D of dry black-marls is approximately 1450 kg m^{-3} (Maquaire et al., 2003).

Before computing the amplitude at the source and the energy of the seismic signals generated by impacts, we first selected the seismic signals with the following criteria. We excluded the seismic signals generated when i) sliding of the blocks occurred, ii) the blocks stopped mid-slope and iii) more generally when the signal-to-noise ratio was too weak on the seismic stations to perform the computation of the apparent anelastic attenuation parameter B_{ij}. B_{ij} is dependent on the frequency of the seismic waves. Therefore the seismic signals were band-pass filtered between 1 and 50 Hz. This frequency band is chosen because most of the seismic wave energy is not attenuated in this band within the span of the seismic network (Figure 2b and d). For each seismic record selected, we manually picked the peaks corresponding to the impacts on each station. This processing results in a data set of 37 impact seismic signals, coming from 9 out of the 28 launches.

4 Results

4.1 Correlation between dynamic parameters and seismic signal features

From the reconstructed trajectories we inferred the velocity, the momentum and the kinetic energy of the block before each impact (Eq. 1), and the potential energy lost during the block trajectory before impact (Eq. 2). The velocities exhibit a low variability, with values ranging from 6 m s^{-1} to 17 m s^{-1} (Figure 3). We did not find significant correlation between the mass and the impact velocity.

The seismic signal processing yielded the maximum amplitude at the source $A0_{max}$ and the radiated seismic energy E_s at each impact. The average uncertainty on the computation of the maximum amplitude $A0_{max}$, inferred from the standard deviation, and expressed as a percentage of the computed values (i.e. $A0_{max} \pm x\% A0_{max}$), ranges from 7% to 129%, and is 58% in average. Regarding the computation of the radiated seismic energy E_s, the uncertainty, estimated following the same approach, ranges from 55% to 152% of the computed values, and is 86% in average.

We investigated the possible correlations between: 1) the maximum amplitude at the source $A0_{max}$ of the seismic signal and the absolute momentum $|p|$ before the impact; 2) the radiated seismic energy E_s and the potential energy lost E_p; 3) the radiated seismic energy E_s and the kinetic energy E_k before impact; and 4) the radiated seismic energy E_s and the mass m of the blocks. The analysis based on the Hertz's theory of impact conducted by Farin et al. (2015) yielded the parameter
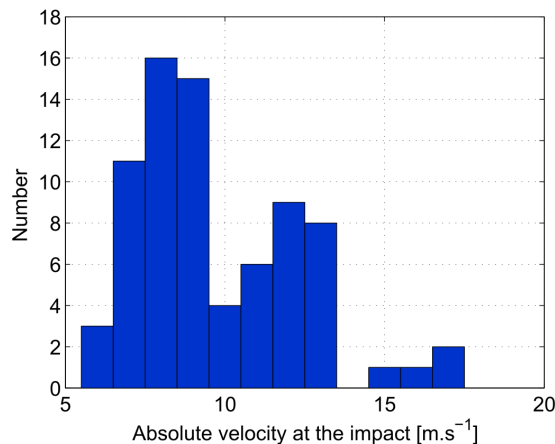
Figure 3. Histogram of the observed absolute velocities before impact.

$mV_z^{13/5}$, with m the mass of the block and V_z the vertical velocity before impact, that should in theory scale with the radiated seismic energy E_s of the seismic signal generated at each impact. However, when investigating this relationship for real single-block rockfalls, they did not found a significant correlation with this parameter. The best correlation they found was with the parameter $mV_z^{0.5}$. We also investigated these two cases with our data set. We computed for each pair of parameters the

5　Spearman rank correlation coefficient ρ and the corresponding $p-values$ (Table 1) (Spearman, 1904) as we assume that the parameters should scale following monotonic laws.

　　The best correlation coefficient ρ has a value of 0.70 for the pair of parameters E_s and E_k. Slightly lower correlation coefficient values are observed between the maximum amplitude $A0_{max}$ and the absolute momentum $|p|$ ($\rho = 0.67$) and the radiated seismic energy E_s and the potential energy E_p ($\rho = 0.68$). The correlation coefficient between the radiated seismic

10　energy E_s and the best empiric parameter $mV_z^{0.5}$ found by Farin et al. (2015) is poorer ($\rho = 0.62$) than the one observed between the radiated seismic energy and the parameter $mV_z^{13/5}$ they derived from the Hertz theory of impact ($\rho = 0.69$). Finally, our results show that there is no correlation between the maximum amplitude $A0_{max}$ and the radiated seismic energy E_s ($\rho = 0.44$) and between the radiated seismic energy E_s and the mass of the blocks m ($\rho = 0.51$). We also investigated other correlations between dynamic parameters and seismic signal features, with the vertical momentum or the vertical kinetic

15　energy for example, but we were unable to improve on the correlations found with the modulus of the dynamic quantities.

　　To characterize the relationships between the parameters that are correlated, we computed the regression lines that best fit the data (Figure 4 and Table 1). According to the theoretical analysis conducted by Farin et al. (2015), the dynamic parameters should scale proportionally with the seismic features. However several studies have shown that linear relationships allow a better fitting of the data gathered from the observation of natural events (e.g. Deparis et al., 2008; Dammeier et al., 2011;

20　Hibert et al., 2011). We computed the regression coefficients of the best fitting lines for the two types of relationships and assessed the quality of the fitting by computing the coefficients of determination R^2.
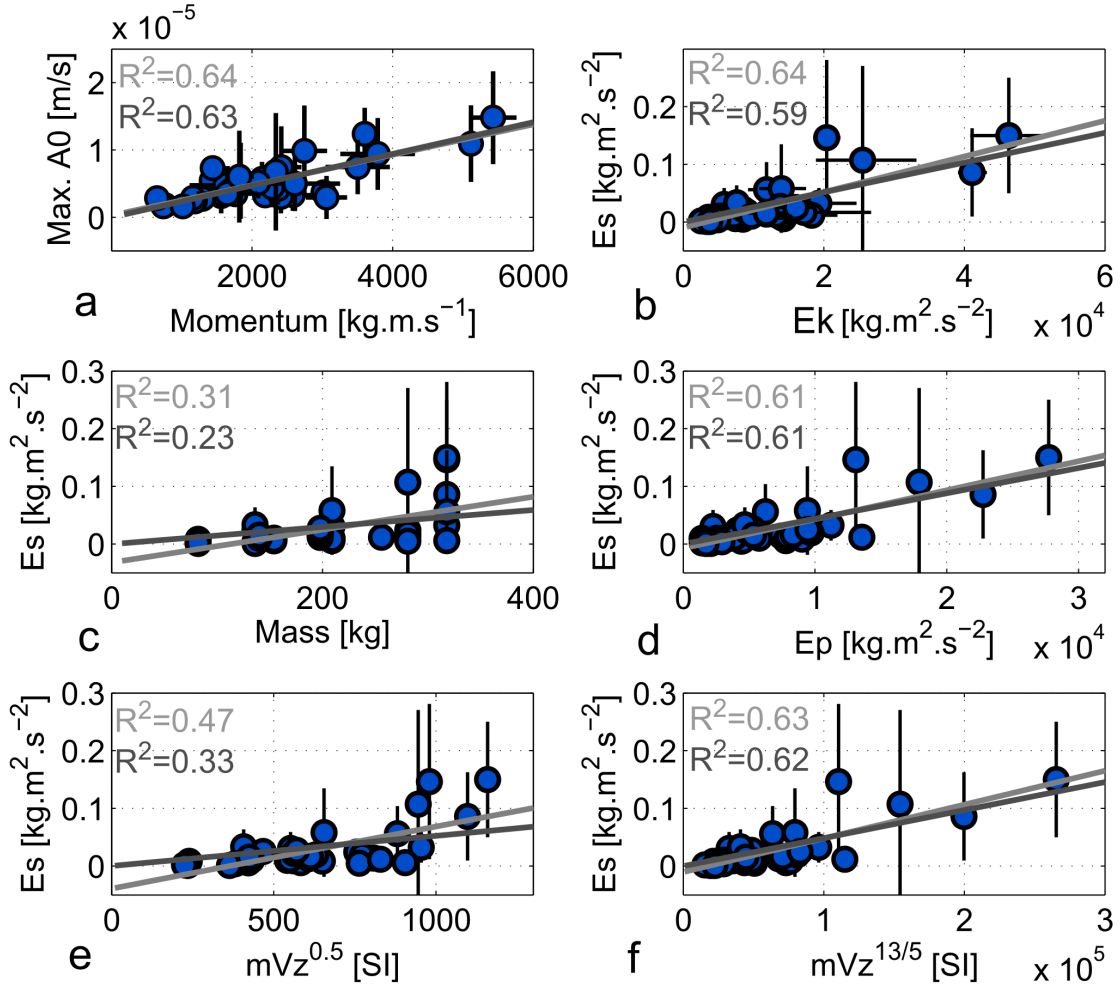
Figure 4. a) Maximum of the amplitude $A0_{max}$, corrected from attenuation, as a function of the average momentum $|p|$ of the block before the impact. Radiated seismic energy E_s of the seismic signal generated at the impact as a function of: b) the kinetic energy before the impact E_k; c) the masses m of the blocks; d) the potential energy lost E_p; e) the parameter $mV_z^{0.5}$; f) the parameter $mV_z^{13/5}$. Errors bars resulting from the computation of the momentum, the kinetic energy and the amplitude at the source are indicated by black lines. For each pair of parameters the light-gray line corresponds to the best regression line computed for a linear relationship and the dark-gray one to the best regression line computed for a proportional relationship.

Overall the R^2 coefficient values do not exceed 0.64 (Table 1). This is caused by a high scattering of the data which comes from the high uncertainties on the computation of the seismic attenuation parameters and hence on the values of $A0_{max}$ and E_s, as shown by the large error bars on Figure 4. The best R^2 coefficients are yielded by the linear regression between the maximum amplitude $A0_{max}$ and the momentum $|p|$, and the radiated seismic energy E_s and the kinetic energy E_k ($R^2 = 0.64$ for both

cases). For the couple of parameters E_s/E_p and $E_s/mV_z^{13/5}$, R^2 coefficients are slightly lower, with values of 0.61 and 0.63 respectively. The regression of each pair of parameters by proportional relationships gives lower values for the coefficient R^2. However the β coefficients of the best linear regressions are close to 0. We assume that linear regressions allow to better accommodate for the scattering of the data than proportional regressions, and that β coefficients are not physically significant.

5 ## 4.2 Retrieving block properties and dynamics from the seismic signal

We have shown that correlations exist between several dynamics quantities and features of the seismic signal generated at each impact. In this section we investigate if these relationships can provide accurate estimates of the mass and the velocity of the blocks, directly from the features of the seismic signals generated by the impacts.

Our results show that the maximum amplitude and the seismic energy are not correlated (Table 1). Hence we can combine
10 the linear relationships inferred for the maximum amplitude and the momentum, and for the radiated seismic energy and the kinetic energy, with the coefficients α and β yielded by the linear regressions. We can express the mass m_i as a function of $A0_{max}$ and E_s as:

$$m_i = \frac{5.9 \times 10^{11}(A0_{max} - 2.50 \times 10^{-7})^2}{(Es + 0.01)}. \tag{7}$$

Using Eq. (7), we computed m_i for each impact of each block for which we were able to compute $A0_{max}$ and E_s, and
15 compared the average estimates of m_i to the measured mass m_r of each block (Table 2). Overall, the inferred masses m_i are close to the real masses m_r of the block. However, the uncertainty on the inferred values is high, especially for blocks for which we have a few number of exploitable impacts and therefore few estimates of $A0_{max}$ and E_s. This may also come from the uncertainties related to the computation of the seismic quantities.

We can also estimate the velocity of the block before each impact using the linear regression and the corresponding coeffi-
20 cients found between the maximum amplitude $A0_{max}$ and the maximum momentum p, or between the seismic energy E_s and the kinetic energy E_k, and with the masses inferred with Eq. 7. We choose to use the linear relationship between the amplitude and the momentum because the uncertainties associated with determining the amplitude at the source are lower than those associated with the radiated seismic energy. The inferred velocity V_i can be computed as:

$$V_i = \frac{A0_{max} - 2.50 \times 10^{-7}}{2.26 \times 10^{-9} m_i}. \tag{8}$$

25 Figure 5a shows the distribution of the absolute difference between the velocities inferred V_i and the velocities V_r derived from the trajectory reconstruction. The values of the difference are comprised between 0.1 and 13.7 $\mathrm{m\,s^{-1}}$, with a median value of 2.4 $\mathrm{m\,s^{-1}}$. We also computed the ratio of the velocity absolute $|V_i - V_r|$ difference over the velocity derived from the trajectory reconstruction V_r (Figure 5b). The majority of the values of the ratio falls below 0.5 (i.e. the difference is less than 50% of the value of the velocity derived from the trajectory reconstruction), and the median ratio is 0.2 (i.e. 20% of the value
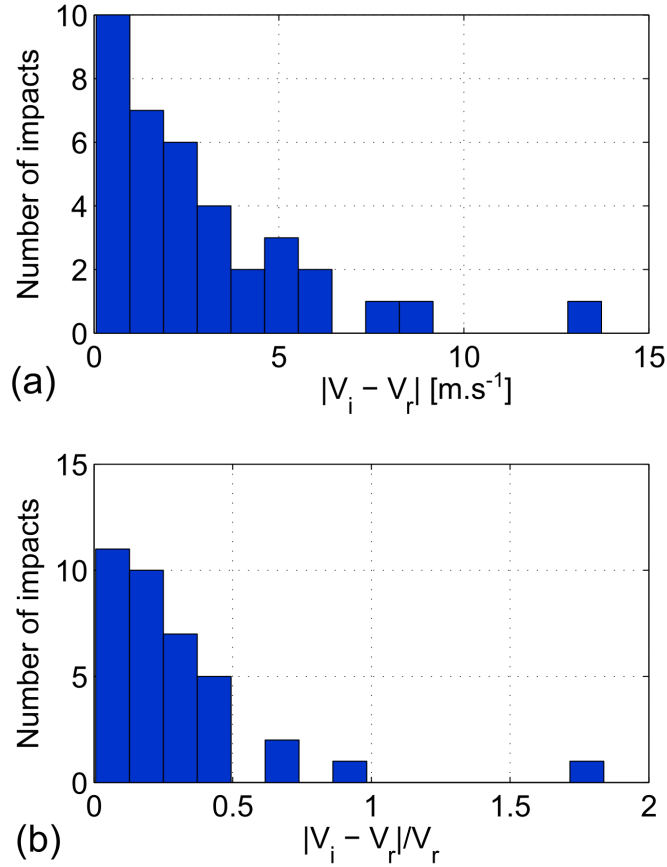30 of the velocity derived from the trajectory reconstruction).

10

Figure 5. a) Histrogram showing the distribution of the difference between the velocity before impact V_i inferred using Eq. 7 and Eq. 8 and the velocity V_r estimated from the video cameras; b) Same as a) but normalized by the value of the velocity V_r estimated via the video cameras.

5 Discussion and conclusion

The Rioux-Bourdoux experiment of controlled single-block rockfalls produced important results to better understand the links between the dynamics of rockfalls and the seismic signal associated. Our results suggest that correlations exist between the seismic signal features and the dynamic quantities of single-block rockfalls. We observed that the maximum amplitude of the seismic signal generated at each impact and the momentum (product of the mass and the velocity) of the blocks are correlated. Our results also suggest that the energy of the seismic radiation released at each impact scales linearly with the potential energy lost and the kinetic energy. Despite large uncertainties, mainly caused by the simple seismic attenuation model used, the scaling

laws found permit to infer realistic values of the masses and the velocities before impact of the blocks from the amplitude and the energy of the seismic signal generated.

We found that the relationship derived from the Hertz's theory of impact proposed by Farin et al. (2015) that links the radiated seismic energy of the signal generated to the parameter $mV_z^{13/5}$ is verified with our data. However the scaling between the seismic energy and the parameter $mV_z^{13/5}$ did not yield significantly better quantitative correlation than the one observed between the radiated seismic energy and the kinetic energy, or between the amplitude at the source and the momentum of the block before impact ($\rho = 0.69, 0.70$ and 0.67 respectively). This confirms the combined role of the mass and the velocity before impacts of the block in the generation of seismic waves, but does not allow us to identify a unique dynamic parameter that would control the seismic signal features. Further analytical and theoretical developments are needed to understand the physical processes that explain these correlations, and ultimately what are the physical parameters that control the characteristics of the seismic signal generated.

An issue that arose from studies on the link between the seismic signals and the dynamics of mass movements is about the energy transfer and more specifically the ratio $R_{s/p}$ between the radiated seismic energy and the potential energy lost. Deparis et al. (2008) found for 10 rockfalls that occurred in the French Alps that this $R_{s/p}$ ratio is comprised between 10^{-5} and 10^{-4}. Vilajosana et al. (2008) have found a $R_{s/p}$ ratio of 10^{-3} for an artificially triggered rockfalls in the Montserrat massif (Spain). In volcanic contexts, Hibert et al. (2011) and Levy et al. (2015) have observed $R_{s/p}$ ratios ranging from 10^{-5} to 10^{-3}. In this study, we found a $R_{s/p}$ ratio between the radiated seismic energy and the potential energy lost of approximately 10^{-6} (Table 1). Interestingly a ratio of the same order is observed between the radiated seismic energy and the kinetic energy. The value of the $R_{s/p}$ ratio is lower than those observed in other contexts. We assume that this might be explained by the nature of the substrate as in our case the rockfalls propagated on unconsolidated soft-rocks, which may absorbed more potential energy (by deformation for example) than consolidated igneous (Hibert et al., 2011; Levy et al., 2015) or metamorphic rocks (Deparis et al., 2008; Vilajosana et al., 2008). Investigating this assumption on the role of the substrate on energy transfer by replicating the experiment of controlled releases of single blocks in other contexts constitutes one of the perspectives of this work.

The relationships found open the possibility to estimate directly the mass and the dynamic parameters of single-block rockfalls from the generated seismic signal. However, we identified several limitations that have to be addressed before considering an operational application of seismology to quantify rockfall properties. First, our results show that better attenuation models are needed to reduce the uncertainties on the computation of the seismic signal features. This could be achieved by deploying denser seismic networks for example. Second, the range of the mass of the blocks used in our experiment spans only one order of magnitude. The behavior of the relationships we found has to be investigated for a larger range of volumes. This again underlines the relevance and the necessity of reproducing similar studies in new contexts.

Finally, our results give a new insight on the processes that generate high-frequency seismic signals associated with rockfalls, landslides, rock-avalanches, and granular flows in general. We show that the maximum amplitude of the seismic signal generated by the impact of a single particle is proportional to its mass and velocity. In a granular flow, a very large quantity of particles interact with themselves and with the substrate at a given time. The magnitude of these impulses imparted on the Earth by each particle might be controlled by the mass and the velocity of the particles within the flow according to the correlations

we observed. The issue is now to understand what controls the dynamics of the particles within the flow and how their complex interactions influence the generation of seismic waves. This should be more thoroughly investigated, using numerical granular flow models for example, and is probably the key to model the high-frequency seismic signal associated with gravitational instabilities in the future.

6   Code and Data availability

The codes and the data used in this study are accessible upon request by contacting C. Hibert (hibert@unistra.fr).

References

Aki, K. and Chouet, B.: Origin of coda waves: source, attenuation, and scattering effects, Journal of geophysical research, 80, 3322–3342, 1975.

Allstadt, K.: Extracting source characteristics and dynamics of the August 2010 Mount Meager landslide from broadband seismograms, Journal of Geophysical Research, 118, 1472–1490, doi:10.1002/jgrf.20110, 2013.

Amitrano, D., Grasso, J. R., and Senfaute, G.: Seismic precursory patterns before a cliff collapse and critical point phenomena, Geophysical Research Letters, 32, 2005.

Burjánek, J., Moore, J. R., Molina, F. X. Y., and Fäh, D.: Instrumental evidence of normal mode rock slope vibration, Geophysical Journal International, 188, 559–569, 2012.

Burtin, A., Hovius, N., Milodowski, D. T., Chen, Y.-G., Wu, Y.-M., Lin, C.-W., Chen, H., Emberson, R., and Leu, P.-L.: Continuous catchment-scale monitoring of geomorphic processes with a 2-D seismological array, Journal of Geophysical Research: Earth Surface, 118, 1956–1974, 2013.

Chen, C.-H., Chao, W.-A., Wu, Y.-M., Zhao, L., Chen, Y.-G., Ho, W.-Y., Lin, T.-L., Kuo, K.-H., and Chang, J.-M.: A seismological study of landquakes using a real-time broad-band seismic network, Geophysical Journal International, 194, 885–898, 2013.

Clouard, V., Athanase, J.-E., and Aubaud, C.: Physical characteristics and triggering mechanisms of the 2009–2010 landslide crisis at Montagne Pelée volcano, Martinique: implication for erosional processes and debris-flow hazards, Bulletin de la Société Géologique de France, 184, 155–164, 2013.

Crampin, S.: Higher modes of seismic surface waves: Second Rayleigh mode energy, Journal of Geophysical Research, 70, 5135–5143, 1965.

Dammeier, F., Moore, J. R., Haslinger, F., and Loew, S.: Characterization of alpine rockslides using statistical analysis of seismic signals, Journal of Geophysical Research, 116, F04 024, doi:10.1029/2011JF002037, 2011.

Dammeier, F., Moore, J. R., Hammer, C., Haslinger, F., and Loew, S.: Automatic detection of alpine rockslides in continuous seismic data using Hidden Markov Models, Journal of Geophysical Research: Earth Surface, 121, 351–371, 2016.

Deparis, J., Jongmans, D., Cotton, F., Baillet, L., Thouvenot, F., and Hantz, D.: Analysis of rock-fall and rock-fall avalanche seismograms in the French Alps, Bulletin of the Seismological Society of America, 98, 1781–1796, doi:10.1785/0120070082, 2008.

Ekström, G. and Stark, C. P.: Simple scaling of catastrophic landslide dynamics, Science, 339, 1416–1419, doi:10.1126/science.1232887, 2013.

Farin, M., Mangeney, A., Toussaint, R., Rosny, J. d., Shapiro, N., Dewez, T., Hibert, C., Mathon, C., Sedan, O., and Berger, F.: Characterization of rockfalls from seismic signal: Insights from laboratory experiments, Journal of Geophysical Research: Solid Earth, 120, 7102–7137, doi:10.1002/2015JB012331, 2015JB012331, 2015.

Favreau, P., Mangeney, A., Lucas, A., Crosta, G., and Bouchut, F.: Numerical modeling of landquakes, Geophysical Research Letters, 37, L15 305, doi:10.1029/2010GL043512, 2010.

Galea, P., D'Amico, S., and Farrugia, D.: Dynamic characteristics of an active coastal spreading area using ambient noise measurements—Anchor Bay, Malta, Geophysical Journal International, 199, 1166–1175, 2014.

Gance, J., Grandjean, G., Samyn, K., and Malet, J.-P.: Quasi-Newton inversion of seismic first arrivals using source finite bandwidth assumption: Application to subsurface characterization of landslides, Journal of Applied Geophysics, 87, 94–106, 2012.

Helmstetter, A. and Garambois, S.: Seismic monitoring of Séchilienne rockslide (French Alps): Analysis of seismic signals and their correlation with rainfalls, Journal of Geophysical Research, 115, F03 016, doi:10.1029/2009JF001532, 2010.

Hertz, H.: Über die Berührung fester elastischer Körper., Journal für die reine und angewandte Mathematik, 92, 156–171, 1882.

Hibert, C., Mangeney, A., Grandjean, G., and Shapiro, N. M.: Slope instabilities in Dolomieu crater, Réunion Island: From seismic signals to rockfall characteristics, Journal of Geophysical Research, 116, F04 032, doi:10.1029/2011JF002038, 2011.

Hibert, C., Grandjean, G., Bitri, A., Travelletti, J., and Malet, J.-P.: Characterizing landslides through geophysical data fusion: Example of the La Valette landslide (France), Engineering Geology, 128, 23–29, 2012.

Hibert, C., Ekström, G., and Stark, C. P.: Dynamics of the Bingham Canyon Mine landslides from seismic signal analysis, Geophysical Research Letters, 41, 4535–4541, doi:10.1002/2014GL060592, 2014a.

Hibert, C., Mangeney, A., Grandjean, G., Baillard, C., Rivet, D., Shapiro, N. M., Satriano, C., Maggi, A., Boissier, P., Ferrazzini, V., and Crawford, W.: Automated identification, location, and volume estimation of rockfalls at Piton de la Fournaise volcano, Journal of Geophysical Research: Earth Surface, 119, 1082–1105, doi:10.1002/2013JF002970, http://dx.doi.org/10.1002/2013JF002970, 2014b.

Hibert, C., Stark, C. P., and Ekström, G.: Seismology of the Oso-Steelhead landslide, Nat. Hazards Earth Syst. Sci. Discuss., pp. 7309–7327, 2014c.

Hibert, C., Ekström, G., and Stark, C. P.: The relationship between bulk-mass momentum and short-period seismic radiation in catastrophic landslides, Submitted to Journal of Geophysical Research: Earth Surface, 2017.

Levy, C., Jongmans, D., and Baillet, L.: Analysis of seismic signals recorded on a prone-to-fall rock column (Vercors massif, French Alps), Geophysical Journal International, 186, 296–310, 2011.

Levy, C., Mangeney, A., Bonilla, F., Hibert, C., Calder, E. S., and Smith, P. J.: Friction weakening in granular flows deduced from seismic records at the Soufrière Hills Volcano, Montserrat, Journal of Geophysical Research: Solid Earth, 120, 7536–7557, 2015.

Maquaire, O., Malet, J.-P., Remaître, A., Locat, J., Klotz, S., and Guillon, J.: Instability conditions of marly hillslopes: towards landsliding or gullying? The case of the Barcelonnette Basin, South East France, Engineering Geology, 70, 109–130, 2003.

Moretti, L., Mangeney, A., Capdeville, Y., Stutzmann, E., Huggel, C., Schneider, D., and Bouchut, F.: Numerical modeling of the Mount Steller landslide flow history and of the generated long period seismic waves, Geophysical Research Letters, 39, L16 402, doi:10.1029/2012GL052511, 2012.

Norris, R. D.: Seismicity of rockfalls and avalanches at three Cascade Range volcanoes: Implications for seismic detection of hazardous mass movements, Bulletin of the Seismological Society of America, 84, 1925–1939, 1994.

Panzera, F., D'Amico, S., Lotteri, A., Galea, P., and Lombardo, G.: Seismic site response of unstable steep slope using noise measurements: the case study of Xemxija bay area, Malta, Natural Hazards and Earth System Sciences, 12, 3421, 2012.

Schneider, D., Bartelt, P., Caplan-Auerbach, J., Christen, M., Huggel, C., and McArdell, B. W.: Insights into rock-ice avalanche dynamics by combined analysis of seismic recordings and a numerical avalanche model, Journal of Geophysical Research, 115, F04 026, doi:10.1029/2010JF001734, 2010.

Spearman, C.: The proof and measurement of association between two things, The American journal of psychology, 15, 72–101, 1904.

Tripolitsiotis, A., Daskalakis, A., Mertikas, S., Hristopulos, D., Agioutantis, Z., and Partsinevelos, P.: Detection of small-scale rockfall incidents using their seismic signature, in: Third International Conference on Remote Sensing and Geoinformation of the Environment, pp. 953 519–953 519, International Society for Optics and Photonics, 2015.

Vilajosana, I., Suriñach, E., Abellán, A., Khazaradze, G., Garcia, D., and Llosa, J.: Rockfall induced seismic signals: case study in Montserrat, Catalonia, Natural Hazards and Earth System Sciences, 8, 805–812, doi:10.5194/nhess-8-805-2008, http://www.nat-hazards-earth-syst-sci.net/8/805/2008/nhess-8-805-2008.html, 2008.

Yamada, M., Matsushi, Y., Chigira, M., and Mori, J.: Seismic recordings of landslides caused by Typhoon Talas (2011), Japan, Geophysical Research Letters, 39, L13 301, doi:10.1029/2012GL052174, 2012.

Yamada, M., Kumagai, H., Matsushi, Y., and Matsuzawa, T.: Dynamic landslide processes revealed by broadband seismic records, Geophysical Research Letters, 40, 2998–3002, doi:10.1002/grl.50437, 2013.

Zimmer, V. L. and Sitar, N.: Detection and location of rock falls using seismic and infrasound sensors, Engineering Geology, 193, 49–60, 2015.

Parameters (X,Y)	Spearman correlation		Proportional			linear		
	ρ	$p-values$	α	β	R^2	α	β	R^2
$A0_{max} = \alpha\,|p| + \beta$	0.67	$1.12\,10^{-7}$	$2.35\,10^{-9}$	0	0.63	$2.26\,10^{-9}$	$2.50\,10^{-7}$	0.64
$E_s = \alpha\,E_p + \beta$	0.68	$6.75\,10^{-6}$	$4.40\,10^{-6}$	0	0.61	$5.04\,10^{-6}$	-0.01	0.61
$E_s = \alpha\,E_k + \beta$	0.70	$3.01\,10^{-6}$	$2.59\,10^{-6}$	0	0.59	$3.09\,10^{-6}$	-0.01	0.64
$E_s = \alpha\,m + \beta$	0.51	$1.3\,10^{-3}$	$1.48\,10^{-4}$	0	0.23	$2.85\,10^{-4}$	-0.03	0.31
$E_s = \alpha\,mV_z^{13/5} + \beta$	0.69	$4.16\,10^{-6}$	$4.86\,10^{-7}$	0	0.62	$5.85\,10^{-7}$	-0.01	0.63
$E_s = \alpha\,mV_z^{0.5} + \beta$	0.62	$7.63\,10^{-5}$	$5.24\,10^{-5}$	0	0.33	$1.07\,10^{-4}$	-0.04	0.47
$A0_{max} = \alpha\,E_s + \beta$	0.44	$8.2\,10^{-3}$	-	-	-	-	-	-

Table 1. Spearman correlation coefficients, coefficients of the regression lines for proportional and linear relationships and corresponding coefficient of determination R^2.

Block #	m_r [kg]	m_i [kg]	std.	Nbr. impacts
9	281	198	56	5
1	318	334	71	6
4	209	208	115	7
35	82	84	68	3
33	256	97	-	1
22	154	171	146	3
20	198	211	39	6
17	136	181	118	4
13	140	270	162	2

Table 2. Comparison between the real mass m_r of the blocks and the average inferred masses m_i computed with Eq. 7.